



<b>Title</b>	Inherent control of growth, morphology and defect formation in germanium nanowires
<b>Author(s)</b>	Biswas, Subhajt; Singha, Achintya; Morris, Michael A.; Holmes, Justin D.
<b>Publication date</b>	2012-10-15
<b>Original citation</b>	Biswas, S., Singha, A., Morris, M. A. and Holmes, J. D. (2012) 'Inherent Control of Growth, Morphology, and Defect Formation in Germanium Nanowires', Nano Letters, 12(11), pp. 5654-5663. doi: 10.1021/nl302800u
<b>Type of publication</b>	Article (peer-reviewed)
<b>Link to publisher's version</b>	<a href="https://pubs.acs.org/doi/abs/10.1021/nl302800u">https://pubs.acs.org/doi/abs/10.1021/nl302800u</a> <a href="http://dx.doi.org/10.1021/nl302800u">http://dx.doi.org/10.1021/nl302800u</a> Access to the full text of the published version may require a subscription.
<b>Rights</b>	© 2012 American Chemical Society. This document is the Accepted Manuscript version of a Published Work that appeared in final form in Nano Letters, copyright © American Chemical Society after peer review and technical editing by the publisher. To access the final edited and published work see <a href="https://pubs.acs.org/doi/abs/10.1021/nl302800u">https://pubs.acs.org/doi/abs/10.1021/nl302800u</a>
<b>Item downloaded from</b>	<a href="http://hdl.handle.net/10468/6757">http://hdl.handle.net/10468/6757</a>

Downloaded on 2018-09-21T13:40:48Z

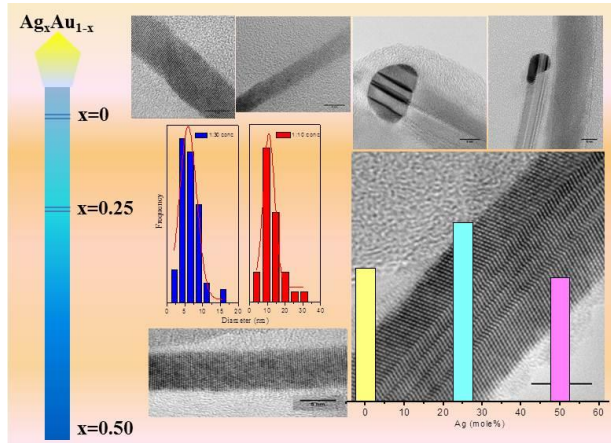
# **Inherent Control of Growth, Morphology and Defect Formation in Germanium Nanowires**

*Subhajit Biswas<sup>†</sup>, Achintya Singha<sup>§</sup>, Michael A. Morris<sup>†,ϕ</sup> and Justin D. Holmes<sup>†,ϕ,\*</sup>*

<sup>†</sup>Materials Chemistry & Analysis Group, Department of Chemistry and the Tyndall National Institute, University College Cork, Cork, Ireland. <sup>ϕ</sup>Centre for Research on Adaptive Nanostructures and Nanodevices (CRANN), Trinity College Dublin, Dublin 2, Ireland. <sup>§</sup>Department of Physics, Bose Institute, Kolkata-700009, India.

\*To whom correspondence should be addressed: Tel: +353 (0)21 4903608; Fax: +353 (0)21 4274097; E-mail: j.holmes@ucc.ie

## Table of Contents Graphic:



**ABSTRACT:** The use of bi-metallic alloy seeds for growing one-dimensional nanostructures has recently gained momentum amongst researchers. The compositional flexibility of alloys provides the opportunity to manipulate the chemical environment, reaction kinetics and thermodynamic behavior of nanowire growth, in both the eutectic and sub-eutectic regimes. This article describes for the first time the role of  $Au_xAg_{1-x}$  alloy nanoparticles in defining the growth characteristics and crystal quality of solid-seeded Ge nanowires via a supercritical fluid growth process. Enhanced diffusivity of Ge in the alloy seeds, compared to pure Ag seeds, and slow interparticle diffusion of the alloy nanoparticles allows realization of high-aspect ratio nanowires with diameters below 10 nm, via a seeded bottom-up approach. Also detailed is the influence the alloyed seeds have on the crystalline features of nanowires synthesized from them, *i.e.* planar defects. The distinctive stacking fault energies, formation enthalpies and diffusion chemistries of the nanocrystals result in different magnitudes of {111} stacking faults in the seed particles and the subsequent growth of <112>-oriented nanowires with radial twins through a *defect transfer* mechanism; with the highest number twinned Ge nanowires obtained using  $Ag_{0.75}Au_{0.25}$  growth seeds. Employing alloy nanocrystals for intrinsically dictating the growth behavior and crystallinity of nanowires could open up the possibility of engineering nanowires with tuneable structural and physical properties.

**KEYWORDS:** Germanium, nanowire, supercritical fluid-solid-solid (SFSS) growth,  $Ag_xAu_{1-x}$  alloy, twin, electron microscopy

Group 14 semiconductor nanowires have a vast range of potential applications, including chemical and biological sensing, computing, optoelectronics and

photovoltaics.<sup>1-9</sup> Germanium (Ge) is of particular interest for high speed nanoelectronic applications due to its low band gap energy (0.67 eV at room temperature) and high hole mobility (2000-4000 cm<sup>2</sup> V<sup>-1</sup> s<sup>-1</sup>).<sup>10</sup> High quality Ge nanowires with narrow diameter distributions are commonly grown using solid growth promoters, *e.g.* Ni, in a bottom-up synthetic approach.<sup>11-12</sup> The generation of crystal defects in the form of lamellar twins in nanowires is significant due to the alteration of the electron wavefunction at these defects, giving rise to a change in their band gap energy and electrical properties.<sup>13-14</sup> Also, band gap engineering via strain modulation is gaining interest among researchers.<sup>15-</sup>  
<sup>16</sup> Adding twinning defects into nanowires can serve as a means to induce strain<sup>17-18</sup>, which in turn will affect their band structure and hence the mobilities of electrons and holes. Solid phase seeding of Group 14 nanowires also provides the opportunity to regulate defect formation in nanowires by transferring information from solid catalyst nanoparticles. Additionally, with increasing attention on alternative catalysts for the solid state growth of Group 14 nanowires, there is a need to investigate new catalyst systems which can function in the sub-eutectic regime, providing improved growth/diameter control, superior governing of crystal orientation and crystal defects and increased purity of growth materials. Usually bottom-up synthesis using solid phase catalysts allows control over the aspect ratio, diameter and structure of one-dimensional (1D) crystals, through the control over external parameters such as precursor feedstock, temperature, operating pressure and precursor flow rate.<sup>7, 19-23</sup> Superior control over the morphology of nanowires should also be achievable by regulating the constraints within the triple phase growth regime (vapor source-metal collector-semiconductor nanowire) enabling inherent influence over growth limiting factors, such as diffusion and transport

of materials in the collector and triple phase boundary; the chemical environment and reaction kinetics; thermodynamic behavior of the collector seeds *etc.* One of the most feasible ways to manipulate the triple phase growth regime is to manipulate the collector seed (diameter, composition *etc.*), which should readily affect the growth characteristics of nanowires. Varying the composition of two mono-metal components in bimetallic alloy seed particles ( $A_xB_{1-x}$ ), enables governance over the ternary ‘*metal seed particle (A)-metal seed particle (B)-growth material*’ phase characteristics in both eutectic and sub-eutectic regimes. For example, theoretical calculations for Au-Al-Si ternary systems predicts a eutectic temperature for Si with the intermetallic compound AuAl<sub>2</sub> to be at a temperature of 487 °C, whereas Si has a eutectic of 375 and 577 °C with Au and Al respectively.<sup>24</sup> There have been previous reports of employing alloy seeds to provide better control over junction abruptness and growth directionality in Group 14 nanowires and heterostructures,<sup>25-28</sup> including a very recent study by Chou *et al.*<sup>29</sup> who have demonstrated the role of AuAg alloy seeds in governing heterojunctions in Si/Ge nanowires. However, none of these studies have provided a detailed understanding of the suitability of alloy seeds in directing the growth behavior and crystal quality of nanowires in a solid-seeded regime and the implementation of such seeds in realizing “*super-thin*” nanowires with high aspect ratios. Noble metals such as Au and Ag are readily miscible with each other, they do not form intermetallic compounds or go through a phase change upon dissolution.<sup>30</sup> By taking advantage of the well documented Au-Ag-Ge ternary system, control over the growth behavior of Ge nanowires, in the *sub-eutectic phase regime*, is achievable by manipulating the ratio of Au to Ag in the catalytic nanoparticle seeds. Also, by taking advantage of the prompt formation of stacking faults in Ag

nanoparticles, we have previously demonstrated the forceful induction of twin planes in Ge nanowires from twinned seed particles.<sup>31</sup> The density of planar defects in the collector seed particles can potentially be varied by alloying seeds with different intermetallic compositions. Differing amounts of Ag and Au in the alloy nanoparticles will change the stacking fault energy and interparticle diffusion chemistry of the nanoparticles, which in turn can be utilized to vary crystallographic information in the collector seed particles and subsequently the nanowires grown from them, through epitaxial knowledge transfer.<sup>31</sup> To date, systematic manipulation of twin boundary formation in Group 14 nanocrystals has not been reported.

In this article, we highlight the application of  $Ag_xAu_{1-x}$  colloidal nanoparticles as growth promoters for generating 1D Ge nanostructures via a supercritical fluid-solid-solid (SFSS) approach. We demonstrate the successful implementation of alloy nanoparticles in realizing diameter controlled sub-10 nm Ge nanowires with narrow size distributions. How varying the composition of the alloy nanoparticles readily affects nanowire growth, morphology and defect formation, allowing inherent control over their evolution and crystallinity, is further discussed. To the best of our knowledge, manipulation of (i) the growth kinetics of Ge nanowires in a solid-seeded bottom up growth regime and (ii) the quantity of crystal defects in nanowire samples, simply by varying the seed material composition have not previously been reported and open up the possibility of growth and defect engineering in Group 14 nanowires.

Seeding Ge nanowires from alloy nanoparticles allows control over their growth behavior as the solubility and diffusivity of Ge varies with nanoparticle composition. The noble metals Ag, Au and Al form simple binary phases with Ge, *i.e.* they do not form “metal-Ge” line compounds such as the formation of  $\text{Cu}_3\text{Ge}$  as is the case with Cu. Also the two component phase diagrams of Au, Ag and Al with Ge all display a “pocket” on the metal rich side of their phase diagrams, implying reasonable solubility of Ge in these metals without the formation of germanide compounds. Alloys of these metals could therefore be used to study the growth behavior of Ge nanowires, as the composition of the seeds will only effect the position of the liquidus and solidus lines and the width of the “pockets”.<sup>24, 32</sup> The very low eutectic temperature of Ge with Au ( $\sim 363\text{ }^\circ\text{C}$ )<sup>32</sup> and Al ( $\sim 525\text{ }^\circ\text{C}$ )<sup>33</sup> provides only a limited composition window for the sub-eutectic growth of Ge nanowires using these metals. Significantly, Au-rich ternary Au-Al-Ge systems will have eutectic temperatures too close to the synthesis temperature for Ge nanowire growth, *i.e.* around  $400\text{ }^\circ\text{C}$ , potentially facilitating liquid-catalyst assisted growth of the nanowires, which was to be avoided in this study. Binary phase diagrams<sup>32</sup> of  $\text{Ag}_x\text{Au}_{1-x}$  ( $x = 1, 0.75, 0.5, 0.25$ ) alloys with Ge clearly indicate the existence of eutectics well above the nanowire synthesis temperature and the comprehensible solubility and diffusivity of Ge into these metal alloys (Figure S1, Supporting Information), enabling the use of  $\text{Ag}_x\text{Au}_{1-x}$  alloy seeds as growth promoters for Ge nanowires. These alloy seeds do not form a eutectic melt at the synthetic temperature of  $400\text{ }^\circ\text{C}$  for all possible combinations of Au and Ag, keeping the growth conditions in the sub-eutectic regime.



Dodecanethiol-stabilized  $\text{Ag}_x\text{Au}_{1-x}$  alloy nanoparticles were synthesized by co-reducing a mixture of chloroauric acid ( $\text{HAuCl}_4$ ) and silver nitrate ( $\text{AgNO}_3$ ) in a chloroform/water biphasic solution.<sup>34</sup> The nanoparticles were precipitated with ethanol and re-dispersed in toluene for further use. Figures 1(a)-(c) show transmission electron microscopy (TEM) images of  $\text{Ag}_x\text{Au}_{1-x}$  ( $x = 1, 0.75, 0.5$ ) nanoparticle seeds, with mean diameters close to 4 nm. As the focus of this study was on the solid phase seeding of Ge nanowires,  $\text{Ag}_{0.25}\text{Au}_{0.75}$  nanoparticles were not included in this study as depression of their eutectic point, due to nanosize effects,<sup>35</sup> could lower the eutectic temperature (467 °C for bulk) of the Ge- $\text{Ag}_{0.25}\text{Au}_{0.75}$  system close to the synthesis temperature. Figure 1(d) shows the absorbance spectra of as-synthesized  $\text{Ag}_x\text{Au}_{1-x}$  nanoparticles; a single surface plasmon resonance (SPR) peak was observed for all of the nanoparticle compositions studied. The SPR peak red shifted as the composition of the nanoparticles became richer in Au, suggesting that the formation of  $\text{Ag}_x\text{Au}_{1-x}$  alloy nanoparticles, rather than the growth of core/shell-structured Ag/Au and Au/Ag, or mixtures of Au and Ag, nanoparticles. Energy dispersive X-ray analysis (EDX) analysis also confirmed the presence of both Ag and Au in the alloy nanoparticles; with Ag:Au ratios equivalent to the molar ratios of the Ag and Au salts from which they were synthesized (Figure S2, Supporting Information). These small colloidal alloy nanoparticles were deposited onto silicon substrates and dried at 180 °C under vacuum, leading to desorption of the surfactant molecules from the surface of the particles. The native oxide layer on the Si substrate also played a role in the pre-alignment of the nanoparticles, with respect to the silicon lattice prior to Ge nanowire growth, as the four fold symmetry of hydrogen-

terminated Si(001) surfaces can force multiple orientations of Ag(111) particles with three fold symmetry.<sup>36</sup>

A supercritical-fluid-solid-solid (SFSS) approach, using toluene as the supercritical fluid phase, was adopted for growing the Ge nanowires on the surface of Si (001) substrates. Diphenyl germane was used as the Ge source in the reactions and the nanoparticle concentration in each case was fixed at  $40 \mu\text{mole cm}^{-3}$ . As anticipated from the phase diagram, the effective growth of Ge nanowires was achieved for different alloy nanoparticle seeds after a 3 hr growth time, as shown in the scanning electron microscopy (SEM) images in Figures 2(a) and (b), for both  $\text{Ag}_{0.75}\text{Au}_{0.25}$  and  $\text{Ag}_{0.50}\text{Au}_{0.50}$  seeds. The diameters of the nanowires synthesized ranged in diameter between 10-40 nm for both seed types, whereas the lengths of the nanowires were in the order of several micrometers. High resolution TEM images (Figures 2(c) and (d)) of Ge nanowires grown from  $\text{Ag}_{0.75}\text{Au}_{0.25}$  seeds and their corresponding fast Fourier transformation (FFT) patterns, exhibited a bulk diamond cubic crystal structure (PDF 04-0545), with  $\langle 110 \rangle$  and  $\langle 111 \rangle$  growth directions, which is the most commonly reported growth axis for Ge nanowires in this diameter range. Figure 2(e) shows a TEM image of an alloy metal tip at the end of a synthesized Ge nanowire, with a lattice spacing of 0.238 nm, which is comparable to the {111} face centered cubic (fcc) lattice packing of Ag or Au crystals (PDF 04-0783 for Ag and 04-0784 for Au). EDX analysis of the metal tips (Figure 2(f) and Figure S3, Supporting Information), shown in the dark-field scanning transmission electron microscopy (STEM) images, confirmed the presence of both Ag and Au (mean values: 70.4 % Ag and 29.6 % Au for  $\text{Ag}_{0.75}\text{Au}_{0.25}$  seeds and 54.5 % Ag and 45.5 % Au

for  $\text{Ag}_{0.50}\text{Au}_{0.50}$  seeds), in similar ratios to the composition of the starting nanoparticles. The very low Ge concentration ( $\sim 1\%$ ) at the metal tips (Figure S3, Supporting Information) implies that the growth of the Ge nanowires occurred via a solid state growth mechanism.

Low concentrations ( $8\ \mu\text{mole cm}^{-3}$ ) of  $\text{Ag}_x\text{Au}_{1-x}$  nanoparticles were used to probe the kinetics of Ge nanowire growth from the alloy seeds. As significant melting point depression (calculated using the bond energy model<sup>37</sup>, Figure S4 Supporting Information) and fast diffusion kinetics of small metal alloy nanoparticles ( $< 2.5\ \text{nm}$ ) could lead to uncontrolled liquid-like inter-particle fusion, dilute solutions of larger nanoparticles ( $\geq \sim 4\ \text{nm}$ ) were used in this part of the study. Prior to Ge nanowire growth, these alloy nanoparticles were annealed for 2 hr in supercritical toluene at a synthesis temperature of  $400\ ^\circ\text{C}$  and pressure of 21 MPa respectively, where the nanoparticles fused together to form larger crystals with superior adhesion to the silicon substrates (Figure S5, Supporting Information). Below the melting point of the nanoparticles, coalescence was mainly driven by surface diffusion leading to the formation of large seed particles. A difference in the mean diameter between pure Ag and different alloy  $\text{Ag}_x\text{Au}_{1-x}$  growth seeds was clearly evident after annealing. Coalescence of Ag nanoparticles produced seeds with a mean diameter of  $\sim 30\ \text{nm}$  ( $\pm 3.1$ ), whilst annealing of the alloy nanoparticles generated nanocrystals with a mean diameter 13 nm, with much narrower size distributions (standard deviation of  $\pm 2.1$  and  $\pm 1.8$  for  $\text{Ag}_{0.75}\text{Au}_{0.25}$  and  $\text{Ag}_{0.50}\text{Au}_{0.50}$  seeds respectively), implying slower diffusion kinetics of the metal alloy nanoparticles on the surface of Si substrates. Nichols<sup>38</sup> previously reported that the sintering time of two

equally sized spheres in contact was proportional to  $r^4T/B$ , where  $r$  and  $T$  are the particle radius and temperature respectively and  $B$  is a constant which is proportional to surface energy and diffusivity ( $D$ ). The diffusivity ( $D$ ) temperature relationship can be modeled using the Boltzmann-Arrhenius expression,  $D = D_o \exp(-E_a/RT)$ , where  $D_o$  is the pre-exponential diffusion coefficient,  $E_a$  is the activation energy which is proportional to  $T_m$  (melting point of material in bulk) and  $R$  is the universal gas constant. The surface energy contribution of these metals is sufficiently small when determining the coalescence probability of the nanoparticles, compared to the influence of diffusivity, because of the exponential dependence of diffusivity on the temperature and melting point of nanoparticles. So the faster coalescence for pure Ag nanoparticles can be attributed to the rapid self-mobility of Ag atoms, due to its lower melting point compared to the alloys. After 45 min growth, using similar experimental parameters for all three nanoparticle seeds, Ge nanowires of different mean lengths were obtained, as determined by SEM analysis (Figures 3(a) to (c)). Accurate measurements of Ge nanowire lengths by SEM and TEM analysis revealed that the mean lengths varied from  $\sim 125$  nm for Ag-seeds to approximately  $2 \mu\text{m}$  for  $\text{Ag}_{0.50}\text{Au}_{0.50}$  seeds, whereas a mean length of around 500 nm was observed for  $\text{Ag}_{0.75}\text{Au}_{0.75}$  seeds (Figure 3(d)). The mean diameters of the nanowires produced from the alloy seeds were similar to the diameters of the starting annealed seed particles, implying superior size retention of the seed particles with Ge uptake during nanowire growth (inset of Figures 3(b) and (c)). For example, the mean diameter of  $\text{Ag}_{0.50}\text{Au}_{0.50}$  growth seeds prior to nanowire growth was  $13.1 \pm 1.8$  nm, whereas nanowires grown from them had a mean diameter of  $13.3 \pm 2.2$  nm. Surprisingly, the mean diameter of Ge nanowires synthesized from pure Ag seeds was

smaller (mean diameter  $16.3 \pm 3.4$  nm) than the annealed Ag growth seed particles (Figure 3(a) inset). This downsizing of the mean nanowire diameter from the initial annealed Ag growth seeds implies non-participation of the large ( $>20$  nm) seed particles in nanowire growth over a short growth time period (45 min). This observation is probably due to the increased diffusion pathway for Ge species in the large Ag seeds causing a longer incubation time and resulting in slower growth kinetics. Preservation of the radial dimensions of the alloy seed particles during nanowire growth also confirms the occurrence of solid seeded growth, as the formation of liquid eutectics would cause uncontrolled interparticle diffusion and nanowires with larger mean diameters and wider size distributions. Assuming solid state growth of the nanowires to be diffusion-controlled, rather than a supersaturation limited process, Ge species diffuse through the metal catalyst to the metal-semiconductor interface to maintain the growth of the nanowires. By applying Zener's<sup>39</sup> diffusion model for 1D growth, which incorporates Fick's first law of diffusion, the nanowire growth rate can be represented as  $\frac{dx}{dt}$  where:

$$\frac{dx}{dt} = \frac{D}{A(n_{Ge-s} - n_{Ge-m})} \left( \frac{dn_{Ge-m}}{dx} \right) \quad (1)$$

where  $D$  is the diffusion coefficient of Ge in a metal,  $A$  is the diffusion length,  $(n_{Ge-s} - n_{Ge-m})$  is the concentration difference of Ge in the nanowires and in the metal tip and  $\left( \frac{dn_{Ge-m}}{dx} \right)$  is the concentration gradient of Ge in the metal tip from the source-metal interface to the metal semiconductor interface. Due to the very low solid solubility of Ge in the metal tips (2-3 at. %), the Ge concentration difference ( $n_{Ge-s} - n_{Ge-m}$ ) can be assumed to be equal to the concentration of pure germanium. Assuming the maximum

possible concentration gradient, *i.e.*  $(\frac{dn_{Ge-m}}{dx}) = (n_{Ge_s} - n_{Ge_m})$ , equation (1) simplifies to  $\frac{dx}{dt} = \frac{D}{A}$ . Also, assuming the diffusion length of Ge species inside the solid catalyst to be equivalent to the diameter of the spherical nanoparticle seeds at the nanowire tip (mean diameters have been taken in each case as our diffusion length), the diffusion coefficients ( $D$ ) of Ge in Ag, Ag<sub>0.75</sub>Au<sub>0.25</sub> and Ag<sub>0.50</sub>Au<sub>0.50</sub> seeds were calculated to be  $3.4 \times 10^{-13}$ ,  $9.9 \times 10^{-13}$  and  $5.1 \times 10^{-12}$  cm<sup>2</sup> s<sup>-1</sup> respectively. These diffusion coefficients provide a good insight into the mass transfer rate of Ge within the different metal seeds. The faster rate of diffusion of Ge in the alloy seeds compared to pure Ag seeds, is supported by the higher diffusion coefficient of Ge in bulk Au compared to Ag.<sup>40-41</sup> Tuan *et al.*<sup>11</sup> also applied a similar bulk diffusion model for the Ni-seeded growth of Ge nanowires and reported a diffusivity of Ge in Ni as  $4.25 \times 10^{-13}$  cm<sup>2</sup> s<sup>-1</sup> for a 5 nm diameter nanowire. The faster diffusion of Ge inside in the Ag<sub>x</sub>Au<sub>1-x</sub> alloy seeds, even compared to Ni seeded growth, makes them an ideal candidate for growing long and thin nanowires. Surface diffusion of Ge onto the metal seeds has not been accounted for in our calculations, although this mechanism could also provide a pathway for Ge incorporation at the metal-semiconductor interface. However, the presence of Ge in minute quantities in the Ag<sub>x</sub>Au<sub>1-x</sub> metal tips (as shown in the EDX spectra, Figure S3 Supporting Information) confirms the solid solubility of Ge in the alloy seeds and the dominance of a bulk diffusion process.

Solid phase seeding is the preferred approach for growing thin (< 20 nm) Ge nanowires with uniform radial distributions; minimizing the instances of particle aggregation or sintering of the growth promoters compared to a vapor-liquid-solid (VLS)

approach. Although Ni (1453 °C) and Cu (1083 °C) have higher melting points compared to Ag and  $Ag_xAu_{1-x}$  alloys, leading to increased stability against coarsening at commonly used growth temperatures for Ge nanowires, *e.g.* 400 °C, alloying of these materials with Ge during growth changes their phase. For example, Ge incorporation in Ni seeds promotes the formation of nickel germanide and a phase change from fcc to orthorhombic results in a 300-400 % increase in dimensions.<sup>12</sup> The increased diffusion kinetics of Ge in the alloy seeds, compared to frequently used Ni solid seeds, makes them favorable candidates for the growth of diameter-controlled nanowires. The lower tendency of  $Ag_xAu_{1-x}$  alloy nanoparticles to aggregate compared to Ag (due to their higher melting point, Figure S4 in Supporting Information), the fast diffusion kinetics and minimum expansion of the alloy particles with Ge uptake, make these alloy nanoparticles suitable candidates to promote the growth of very thin and long nanowires. Similar to pure Ag seeds, only a small expansion of the fcc lattice with a 2-3 % incorporation of Ge is expected for the  $Ag_xAu_{1-x}$  alloy seeds (Figure S5, Supporting Information).  $Ag_{0.75}Au_{0.25}$  nanoparticles were selected as a growth promoter for thin Ge nanowires at a synthesis temperature of 390 °C, as the eutectic temperature of Ge in bulk  $Ag_{0.75}Au_{0.25}$  (612 °C) is considerably higher than the eutectic temperature of Ge in bulk  $Ag_{0.50}Au_{0.50}$  (542 °C), hence avoiding the possibility of supercritical fluid-liquid-solid (SFLS) growth and the generation of large diameter nanowires.  $Ag_{0.75}Au_{0.25}$  nanoparticles with a mean diameter of 2.5 nm (Figure S6, Supporting Information), and concentrations of 4.0  $\mu\text{mole cm}^{-3}$  and 1.3  $\mu\text{mole cm}^{-3}$  were used for the growth of thin Ge nanowires, as nanoparticles tend to aggregate, cluster and adsorb on surfaces at higher concentrations.<sup>42</sup> Figure 4(a) shows an SEM image of fairly long ( $\geq 2 \mu\text{m}$ ) nanowires grown from  $Ag_{0.75}Au_{0.25}$  seeds at

a concentration of  $4.0 \mu\text{mole cm}^{-3}$ . A few examples of super-thin nanowires, with diameters  $< 10 \text{ nm}$ , are shown in the TEM images in Figures 4(b)-(d) and also in Figure S7 (Supporting Information). Figure 4(e) displays histograms of the diameter distributions of Ge nanowires, with mean diameters of  $6.0 (\pm 2.4) \text{ nm}$  and  $10.1 (\pm 3.2) \text{ nm}$ , synthesized from  $\text{Ag}_{0.75}\text{Au}_{0.25}$  seeds at nanoparticle concentration of  $1.3 \mu\text{mole cm}^{-3}$  and  $4 \mu\text{mole cm}^{-3}$ ; respectively. These data confirm the successful employment of alloy seeds to grow sub-10 nm nanowires with high aspect ratio in a seeded bottom-up growth approach.

The epitaxial transfer of information, in the form of planar defects, from solid Ag nanoparticles to Ge nanowires has already been demonstrated.<sup>31</sup> Ag nanoseeds can act as preferred growth promoters as they obey the prerequisites for defect transfer: (a) the energy for twin formation in the nanoparticle is moderate, (b) they remain in a solid phase during nanowire growth and (c) there is little change in the structure and lattice constant of the nanoparticles with Ge uptake. Although Au seeds can be ruled out as a growth promoters for transferring defects into Ge nanowires, due to a low melting liquid eutectic, where the solid-liquid transition can be as low as  $280 \text{ }^\circ\text{C}$ , alloys of Au and Ag can serve as a perfect growth initiator for defect generation as they abide the preconditions perfectly. An adequate amount of stacking faults in the solid seeds creates preferential nucleation of  $\langle 112 \rangle$  oriented twinned nanowires. Normally the nucleation centers for twinning at nanoparticle-nanowire interfaces are positions of highly localized strain in the lattice<sup>43</sup> which could be due to stacking faults at the interface between metal seeds and growing nanowires. Usually twinning defects formed during nucleation in



metal seed-semiconductor nanowire interfaces provides a preferential addition site at the triple phase boundary for diffusing species and maintaining subsequent growth in the  $\langle 112 \rangle$  direction.<sup>31</sup> Also defect sites in the seed particles can act as a favored diffusion pathway for Ge atoms to be attached at the triple phase boundary.<sup>44</sup> After the nucleation of twins at a metal seed-semiconductor interface, during the layer-by-layer growth of a nanowire, ledge nucleation remains immobilized at the twinning boundary, thus preventing access of Ge adatoms to low energy  $\{111\}$  facets, promoting the propagation of twin planes along the nanowire axes.<sup>43</sup> A detailed discussion on *defect transfer* from seed particles to nanowires and the propagation of the twinning boundaries into the nanowire was presented in our previous work.<sup>31</sup> As expected,  $Ag_xAu_{1-x}$  seeds encourage the growth of large numbers of axially twinned nanowires. The regular appearance of twin planes in the  $Ag_xAu_{1-x}$  particles, and the corresponding Ge nanowires grown from them, is shown in Figure 5(a) and also in Figure S8 (Supporting Information). The images depict the interaction of the defects in the seed particles and the Ge nanowires from their identical contrast patterns, due to their orientation relative to the impinging electron beam. High resolution TEM images and corresponding FFT patterns shown in Figures 5(b) and (c), clearly illustrate the formation of  $\{111\}$  twin planes with a  $\langle 112 \rangle$  growth axis. The formation of twin boundaries on low index planes is associated with a low surface energy at the interface between the twin and the parent crystal. The probability of forming planar defects in the seed particles as a function of Ag and Au composition, *i.e.* Ag,  $Ag_{0.50}Au_{0.50}$ ,  $Ag_{0.75}Au_{0.25}$ , should vary, allowing the distribution of defects in the growing Ge nanowires to be manipulated. TEM investigations ( $> 200$  nanowires studied for each sample) suggested that around 36 % and 32 % of the total

nanowires were  $\langle 112 \rangle$  directed twinned nanowires for Ag and  $\text{Ag}_{0.50}\text{Au}_{0.50}$  seeds respectively, whereas around 46 % of twinned nanowires were obtained for  $\text{Ag}_{0.75}\text{Au}_{0.25}$  seeds (Figure 5(d)). The mean diameters of axially twinned and single crystalline Ge nanowires grown from a particular seed were similar, *i.e.* with  $\text{Ag}_{0.75}\text{Au}_{0.25}$  seeds the mean diameter of non-defective and twinned nanowires were 19.0 ( $\pm 4.2$ ) nm and 18.1 ( $\pm 4.8$ ) nm respectively (Figure S8, Supporting Information), ruling out any critical diameter-dependent twinning, as previously observed with GaAs<sup>45</sup> and GaP<sup>46</sup> nanowires. Another observation was the increased number of  $\langle 110 \rangle$  directed nanowires grown from pure Ag seeds (~ 36 %) compared to the alloy seeds (between 15-20 %), due to the slower growth rate of Ge nanowires with the pure Ag seeds.<sup>47</sup>

The twinning density, which gives an overview of the number of faulty planes in between normal crystalline planes within a nanowire sample, was calculated from X-ray diffraction (XRD) measurements (Figure S9, Supporting Information). The twin density in the overall sample is limited by the number of  $\langle 112 \rangle$  directed twinned nanowires in the sample and the density of twin boundaries in a single nanowire. For  $\text{Ag}_{0.50}\text{Au}_{0.50}$  seeded nanowires the density of twin boundaries in a single nanowire (measured from TEM analysis) increased with increasing nanowire diameter, whilst it remained similar as a function of diameter for pure Ag- seeded growth (Figure S10, Supporting Information). XRD and Raman spectroscopy analysis can provide information on the number of twinned nanowires and the twin density in individual nanowires, allowing an estimation of the overall twin density in the samples. The coherence length ( $D_e$ ) estimated from XRD is not only limited by the crystallite size but also by the deformation fault

probability. The effective particle size can be written in terms of the coherent domain size ( $D$ ) normal to the reflecting planes, deformation and twin probability  $\alpha$  and  $\beta$  and the lattice parameter ( $a$ ), as shown in equation (2) below:<sup>48</sup>

$$\frac{1}{D_e} = \frac{1}{D} + \frac{C_{hkl}(1.5\alpha + \beta)}{a} \quad (2)$$

where the last term,  $\frac{C_{hkl}(1.5\alpha + \beta)}{a}$ , is the fictitious domain size due to faulting ( $C_{hkl}$  is a constant which depends on the reflecting planes). TEM analysis of the Ge nanowire samples confirmed very few or no deformation faults (with planar defects predominantly in the form of twinning), therefore the deformation fault probability ( $\alpha$ ) can be assumed to be zero. The twinning density in the Ge nanowires was consequently found to be  $2.8 \times 10^{-2}$ ,  $3.1 \times 10^{-2}$  and  $2.5 \times 10^{-2}$  for Ag, Ag<sub>0.75</sub>Au<sub>0.25</sub> and Ag<sub>0.50</sub>Au<sub>0.50</sub> seeded nanowires respectively. There is considerable agreement between TEM and XRD results as both techniques indicate pronounced twinning formation in Ge nanowire grown from Ag<sub>0.75</sub>Au<sub>0.25</sub> seeds, although TEM investigations accounts for the numbers of twinned nanowires and XRD measures the density of twin planes in an overall sample, which takes account both the number of twinned nanowires and twin boundary density in individual nanowires. Figure 5(e) shows the micro-Raman spectra of Ge nanowires grown with pure Ag and alloyed Ag<sub>0.75</sub>Au<sub>0.25</sub> and Ag<sub>0.50</sub>Au<sub>0.50</sub> seeds. The first order transverse optical (TO) phonon mode of the crystalline Ge nanowires was red shifted for the Ag<sub>0.75</sub>Au<sub>0.25</sub> seeded samples, with a considerable peak broadening (FWHM increases from 4.6 to 6.4 cm<sup>-1</sup>) relative to the peaks from nanowire samples grown from other seeds. As all of the Raman measurements were performed at room temperature and at

low laser power, the peak shift and broadening observed with the  $\text{Ag}_{0.75}\text{Au}_{0.25}$ -seeded Ge nanowire samples was not due to a temperature effect, *e.g.* sample heating. The Raman peaks were fitted with a phonon confinement model (PCM) (blue lines) with the mean diameters obtained from TEM measurements. The PCM fitted curve showed a profound mismatch with the actual Raman spectrum for the  $\text{Ag}_{0.75}\text{Au}_{0.25}$  seeded nanowires, whereas less prominent mismatches were observed for Raman spectra obtained from  $\text{Ag}_{0.50}\text{Au}_{0.50}$  and Ag-seeded nanowire samples. The existence of twinning defects in the Ge nanowires results in the formation on ‘non-defective’ segments with widths smaller than the diameters of the nanowires. The high density of twin boundaries in the  $\text{Ag}_{0.75}\text{Au}_{0.25}$  seeded nanowires, over the entire diameter range, along with a large number of twinned nanowires in the sample decreases the effective phonon confinement length resulting in a red shifted asymmetrical and broadened Raman peak.<sup>49</sup> The Raman spectra from the  $\text{Ag}_{0.75}\text{Au}_{0.25}$ -seeded nanowires displayed the greatest broadening and a downshift of the phonon mode, compared to the PCM fitted curve, highlighting the high twinning density in  $\text{Ag}_{0.75}\text{Au}_{0.25}$ -seeded nanowires, in agreement with XRD and TEM observations.

Three competing factors are participating in determining the overall defect distribution in the seed particles and the subsequent transfer of these defects into the Ge nanowires: (i) twin energies of the constituent monometals (Au and Ag in this case), which provides insight into the twin energies of alloys formed from them, (ii) the presence of multiple twinned nanoparticles in the as-synthesized samples and (iii) the nature of attachment of these nanoparticles during coalescence upon heating just prior to

nanowire growth. Reported values of twin energies for Ag are between 12-19 mJ m<sup>-2</sup> whereas Au has a twin energy between 21-26 mJ m<sup>-2</sup>.<sup>50</sup> Although these values are well within the thermal energy provided during the synthesis, the relatively lower twin energy of Ag will encourage greater twin formation in Ag and Ag-rich alloy nanoparticle seeds. The phase stability for a bimetallic system can be described by its formation energy ( $\Delta H_f$ ), which is the difference in energy between the final bimetallic systems and monometals used to form them, where the lowest  $\Delta H_f$  value corresponds to the most stable phase. For a  $Ag_xAu_{1-x}$  bimetallic system,  $\Delta H_f$  can be computed using the following equation:  $\Delta H_f = E_{AgAu} - xE_{Ag} - (1 - x)E_{Au}$ , where  $E_{AgAu}$ ,  $E_{Ag}$ , and  $E_{Au}$  are the cohesive energies of the bimetallic system and the pure Ag and Au components respectively, and  $x$  is the atomic concentration. Using the corresponding cohesive energies for each system,  $\Delta H_f$  for bimetallic Au-Ag (for both Ag rich and Au rich alloys) nanoparticles calculated by Qi *et al.*<sup>51</sup> have negative values compared to their monometal counterparts for different multiple twinned particle (MTP) systems, such as decahedral, icosahedral *etc.*, implying a higher probability of forming MTPs in the as-synthesized alloy nanoparticles than in phase pure Ag nanoparticles. As large volumes of twinned crystals can be formed by the coalescence of separately nucleated twinned nanoparticles, enhanced numbers of MTPs in the original colloidal alloy nanoparticle solution will give rise to further twinning in the catalyst seeds upon heating. Also soft interparticle interactions during the coalescence process will encourage a greater twinning in the annealed growth seeds.<sup>52</sup> The higher melting point for Au-rich nanoparticle alloys leads to less prominent interparticle fusion during pre-annealing prior to nanowire growth, resulting in partial coalescence of particles and softer interparticle attachment, giving rise to defects and

more internal stresses. The relatively small amounts of defected nanowires (<10 %) grown from the 2.5 nm  $\text{Ag}_{0.75}\text{Au}_{0.25}$  seeds confirms the role that nanoparticle coalescence plays in determining twinning in the Ge nanowires, as 4 nm  $\text{Ag}_{0.75}\text{Au}_{0.25}$  seeds yielded 46.2 % twinned nanowires. The small (~2.5 nm) particles will interact stronger with each other compared to larger particles (~4 nm) during pre-annealing, due to the exponential dependence of diffusivity with particle size, giving rise to more prominent coalescence and fewer twinning planes in the growth seeds. The lower amount of twinned nanowires produced with smaller particles (~ 2.5 nm) highlights the role nanoparticle diffusion kinetics plays in determining the amount of twinning events in nanowires. The combined effect of twinning energy and coalescence kinetics in defining the defect distribution in the nanowire samples is further validated by the variation in the number of twin planes observed in a single nanowire as a function of diameter, synthesized from different growth seeds (Figure S10, Supporting Information). For Ge nanowires grown from pure Ag seeds, the similar twin boundary densities observed in the nanowires of different diameters is due to the low twinning energy of the Ag growth seeds; as twinning energy is a material property and should be independent of diameter. Whereas for Ge nanowires grown from Au-rich alloy seeds, large catalytic particles form by the soft attachment of smaller nanoparticles during coalescence, resulting in the formation of a sizeable number of twin planes at the interfaces of adjacent nanoparticles, enhancing twin formation in nanowires through *defect transfer*. The participation of different mechanisms in controlling twinning events in Ge nanowire samples, as detailed in this article, should facilitate the discovery of a *ideal* metal seed, with low twinning energy and controlled

grain boundary diffusion, to allow unprecedented control over the number of periodic twinning events in Group IV nanowires.

In summary, a new approach for controlling the growth behavior of Ge nanowires using  $Ag_xAu_{1-x}$  alloy seeds has been demonstrated. With the increased popularity of solid phase seeding amongst researchers in the field, these alloy seeds can act as new growth promoters which also allow control over the growth characteristics of nanowires. The seeding approach described here contributes to the ever challenging target of producing high aspect ratio nanowires. Varying the compositions of the  $Ag_xAu_{1-x}$  alloy seeds facilitates considerable control over the crystal growth limiting factors to produce long and thin (sub-10 nm) Ge nanowires. The superior size retention of the  $Ag_xAu_{1-x}$  seeds upon Ge incorporation during growth (compared to Ni, Cu or Co seeds), the controlled interparticle diffusion of the seeds (compared to Ag seed) and the favorable diffusion kinetics of Ge inside the alloy seeds, makes them highly effective catalysts for forming Ge nanowires with sub-10 nm dimensions. Hence, given the enormous number of metal alloy seed combinations which could be generated, the alloy-seeded approach for growing group 14 semiconductor nanowires is an attractive option for controlling the structure and hence properties of 1D nanostructures. We have also demonstrated a new technique to induce twin boundary formation into a large number of growing nanowires, allowing control over the defect distribution and twin density in the nanowire samples, by varying the composition of the alloy seeds. A high percentage of nanowires with {111} twinning defects were observed for all three seeds employed in our study. Differences in stacking fault energy, formation enthalpy and coalescence chemistry for alloy seeds with

different intermetallic compositions enabled overall control over twin formation in the Ge nanowires. The concept of alloying seed particles to increase or decrease the twinning probability in the seeds, and hence the nanowires grown from them, provides enormous scope to realize large numbers of uniquely twinned crystals in Group 14 nanowires; which in turn will increase the probability of their integration into device architectures. We strongly believe that the work reported in this article opens up the future prospect of defining twinning events, or twinned superlattices, in Group 14 nanowires.

## **ACKNOWLEDGEMENTS**

We acknowledge financial support from Science Foundation Ireland (Grant: 09/IN.1/I2602). This research was also enabled by the Higher Education Authority Program for Research in Third Level Institutions (2007-2011) via the INSPIRE programme.

## **ASSOCIATED CONTENT**

**Supporting Information.** Detailed experimental procedure, characterization techniques, and equipment used, EDX and XRD studies and TEM images of the synthesized Ge nanowires with thin diameter and longitudinal defects and statistical data. This material is available free of charge via the Internet at <http://pubs.acs.org>.



## REFERENCES

- (1) Burchhart, T.; Zeiner, C.; Lugstein, A.; Henkel, C.; Bertagnolli, E.; *Nanotechnology* **2011**, *22*, 035201.
- (2) Garnett, E.; Yang, P. D.; *Nano Lett.* **2010**, *10*, 1082.
- (3) He, R. R.; Gao, D.; Fan, R.; Hochbaum, A. I.; Carraro, C.; Maboudian, R.; Yang, P. D.; *Advanced Materials* **2005**, *17*, 2098.
- (4) Leonard, F.; Talin, A. A.; Swartzentruber, B. S.; Picraux, S. T.; *Physical review letters* **2009**, *102*, 106805.
- (5) Liu, Y.-C. C.; Rieben, N.; Iversen, L.; Sorensen, B. S.; Park, J.; Nygard, J.; Martinez, K. L.; *Nanotechnology* **2010**, *21*.
- (6) Seo, M. H.; Park, M.; Lee, K. T.; Kim, K.; Kim, J.; Cho, J.; *Energy Environ. Sci.* **2011**, *4*, 425.
- (7) Wu, X. Y.; Kulkarni, J. S.; Collins, G.; Petkov, N.; Almecija, D.; Boland, J. J.; Erts, D.; Holmes, J. D.; *Chem. Mat.* **2008**, *20*, 5954.
- (8) Xiang, J.; Lu, W.; Hu, Y. J.; Wu, Y.; Yan, H.; Lieber, C. M.; *Nature* **2006**, *441*, 489.
- (9) Yi, K. S.; Trivedi, K.; Floresca, H. C.; Yuk, H.; Hu, W.; Kim, M. J.; *Nano Lett.* **2011**, *11*, 5465.
- (10) Cor Claeys, E. S. *GERMANIUM-BASED TECHNOLOGIES From Materials to Devices*. First edition ed.; Elsevier: 2007.
- (11) Tuan, H. Y.; Lee, D. C.; Hanrath, T.; Korgel, B. A.; *Chem. Mat.* **2005**, *17*, 5705.
- (12) Barth, S.; Kolesnik, M. M.; Donegan, K.; Krstic, V.; Holmes, J. D.; *Chem. Mat.* **2011**, *23*, 3335.
- (13) Ikonc, Z.; Srivastava, G. P.; Inkson, J. C.; *Surface Science* **1994**, *307*, 880.
- (14) Ikonc, Z.; Srivastava, G. P.; Inkson, J. C.; *Physical Review B* **1995**, *52*, 14078.
- (15) Logan, P.; Peng, X.; *Physical Review B* **2009**, *80*.
- (16) Mitard, J.; De Jaeger, B.; Eneman, G.; Dobbie, A.; Myronov, M.; Kobayashi, M.; Geypen, J.; Bender, H.; Vincent, B.; Krom, R.; Franco, J.; Winderickx, G.; Vrancken, E.; Vanherle, W.; Wang, W.-E.; Tseng, J.; Loo, R.; De Meyer, K.; Caymax, M.; Pantisano, L.; Leadley, D. R.; Meuris, M.; Absil, P. P.; Biesemans, S.; Hoffmann, T.; *Jpn. J. Appl. Phys.* **2011**, *50*.
- (17) Wu, B.; Heidelberg, A.; Boland, J. J.; Sader, J. E.; Sun, X. M.; Li, Y. D.; *Nano Lett.* **2006**, *6*, 468.
- (18) Afanasyev, K. A.; Sansoz, F.; *Nano Lett.* **2007**, *7*, 2056.
- (19) Collins, G.; Kolesnik, M.; Krstic, V.; Holmes, J. D.; *Chem. Mat.* **2010**, *22*, 5235.
- (20) Kodambaka, S.; Tersoff, J.; Reuter, M. C.; Ross, F. M.; *Science* **2007**, *316*, 729.
- (21) Koto, M.; Marshall, A. F.; Goldthorpe, I. A.; McIntyre, P. C.; *Small* **2010**, *6*, 1032.
- (22) Lensch-Falk, J. L.; Hemesath, E. R.; Perea, D. E.; Lauhon, L. J.; *J. Mater. Chem.* **2009**, *19*, 849.
- (23) Simanullang, M.; Usami, K.; Kodera, T.; Uchida, K.; Oda, S.; *Jpn. J. Appl. Phys.* **2011**, *50*.
- (24) Hoch, M.; *Journal of Alloys and Compounds* **1995**, *220*, 27.
- (25) Kang, K.; Gu, G. H.; Kim, D. A.; Park, C. G.; Jo, M. H.; *Chem. Mat.* **2008**, *20*, 6577.
- (26) Connell, J. G.; Al Balushi, Z. Y.; Sohn, K.; Huang, J. X.; Lauhon, L. J.; *J. Phys. Chem. Lett.* **2010**, *1*, 3360.

- (27) Wen, C. Y.; Reuter, M. C.; Bruley, J.; Tersoff, J.; Kodambaka, S.; Stach, E. A.; Ross, F. M.; *Science* **2009**, *326*, 1247.
- (28) Perea, D. E.; Li, N.; Dickerson, R. M.; Misra, A.; Picraux, S. T.; *Nano Lett.* **2011**, *11*, 3117.
- (29) Yi-Chia Chou, C. Y. W., Mark C. Reuter, Dong Su, Eric A. Stach and Frances M. Ross; *ACS Nano* **2012**.
- (30) Hassam, S.; Agren, J.; Gauneescard, M.; Bros, J. P.; *Metallurgical Transactions a-Physical Metallurgy and Materials Science* **1990**, *21*, 1877.
- (31) Barth, S.; Boland, J. J.; Holmes, J. D.; *Nano Lett.* **2011**, *11*, 1550.
- (32) Wang, J.; Liu, Y. J.; Tang, C. V.; Liu, L. B.; Zhou, H. Y.; Jin, Z. P.; *Thermochimica Acta* **2011**, *512*, 240.
- (33) Kagaya, H. M.; Imazawa, K.; Sato, M.; Soma, T.; *Physica B* **1998**, *245*, 252.
- (34) He, S. T.; Xie, S. S.; Yao, J. N.; Gao, H. J.; Pang, S. J.; *Applied Physics Letters* **2002**, *81*, 150.
- (35) Schwalbach, E. J.; Voorhees, P. W.; *Nano Lett.* **2008**, *8*, 3739.
- (36) Li, B. Q.; Zuo, J. M.; *Physical Review B* **2005**, *72*.
- (37) Qi, W. H.; Wang, M. P.; *Materials Chemistry and Physics* **2004**, *88*, 280.
- (38) Nichols, F. A.; *Journal of Applied Physics* **1966**, *37*, 2805.
- (39) Zener, C.; *Journal of Applied Physics* **1949**, *20*, 950.
- (40) Hoffman, R. E.; *Acta Metallurgica* **1958**, *6*, 95.
- (41) Ingrey, S.; Maclaurin, B.; *Journal of Vacuum Science & Technology a-Vacuum Surfaces and Films* **1984**, *2*, 358.
- (42) Min, Y.; Akbulut, M.; Kristiansen, K.; Golan, Y.; Israelachvili, J.; *Nature Materials* **2008**, *7*, 527.
- (43) Dayeh, S. A.; Wang, J.; Li, N.; Huang, J. Y.; Gin, A. V.; Picraux, S. T.; *Nano Lett.* **2011**, *11*, 4200.
- (44) Germain, V.; Li, J.; Ingert, D.; Wang, Z. L.; Pileni, M. P.; *Journal of Physical Chemistry B* **2003**, *107*, 8717.
- (45) Davidson, F. M.; Schricker, A. D.; Wiacek, R. J.; Korgel, B. A.; *Advanced Materials* **2004**, *16*, 646.
- (46) Davidson, F. M.; Wiacek, R.; Korgel, B. A.; *Chem. Mat.* **2005**, *17*, 230.
- (47) Hanrath, T.; Korgel, B. A.; *Small* **2005**, *1*, 717.
- (48) Cohen, J. B.; Wagner, C. N. J.; *Journal of Applied Physics* **1962**, *33*, 2073.
- (49) Li, B. B.; Yu, D. P.; Zhang, S. L.; *Physical Review B* **1999**, *59*, 1645.
- (50) Rosengaard, N. M.; Skriver, H. L.; *Physical Review B* **1993**, *47*, 12865.
- (51) Qi, W. H.; Lee, S. T.; *Journal of Physical Chemistry C* **2010**, *114*, 9580.
- (52) Rupich, S. M.; Shevchenko, E. V.; Bodnarchuk, M. I.; Lee, B.; Talapin, D. V.; *Journal of the American Chemical Society* **2010**, *132*, 289.

## Figures

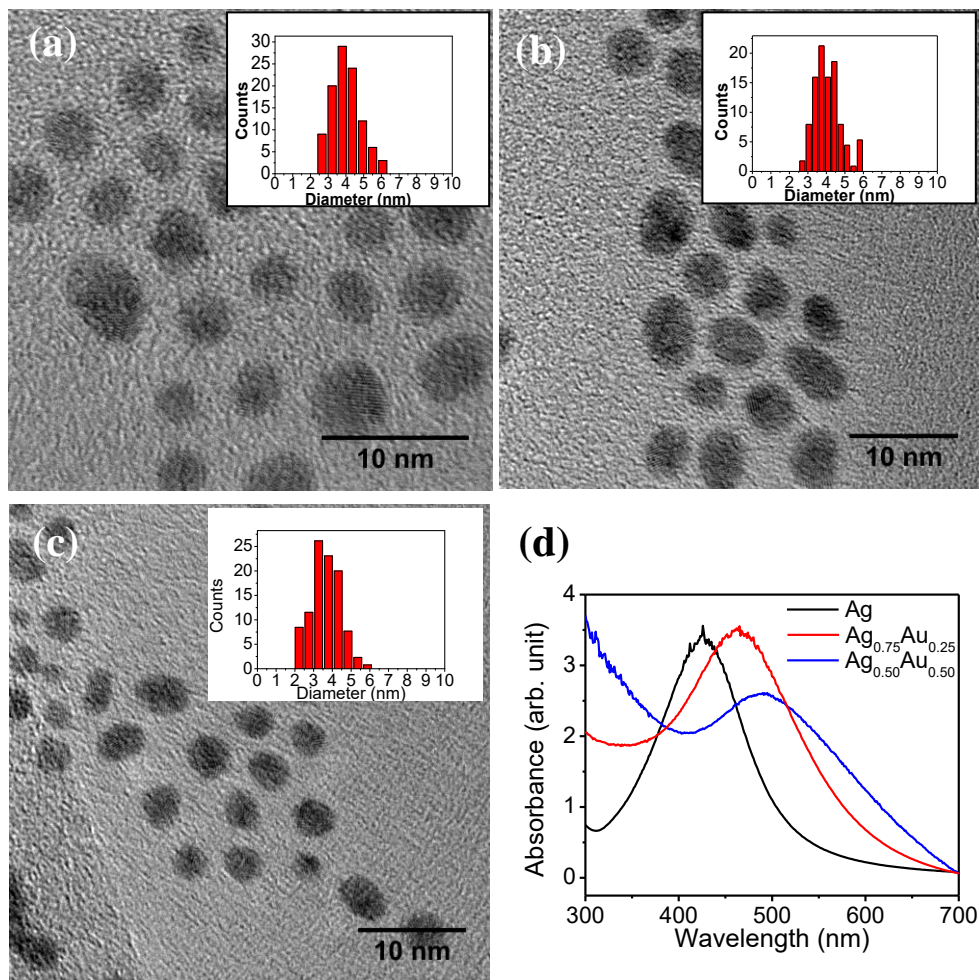


**Figure 1.** TEM images of (a) Ag, (b)  $\text{Ag}_{0.75}\text{Au}_{0.25}$  and (c)  $\text{Ag}_{0.50}\text{Au}_{0.50}$  nanoparticles, with mean diameters of 4 nm. Insets show the particle size distributions. (d) UV-visible spectra of the nanoparticles (a) to (c) displaying a gradual red-shift with increasing Au content.

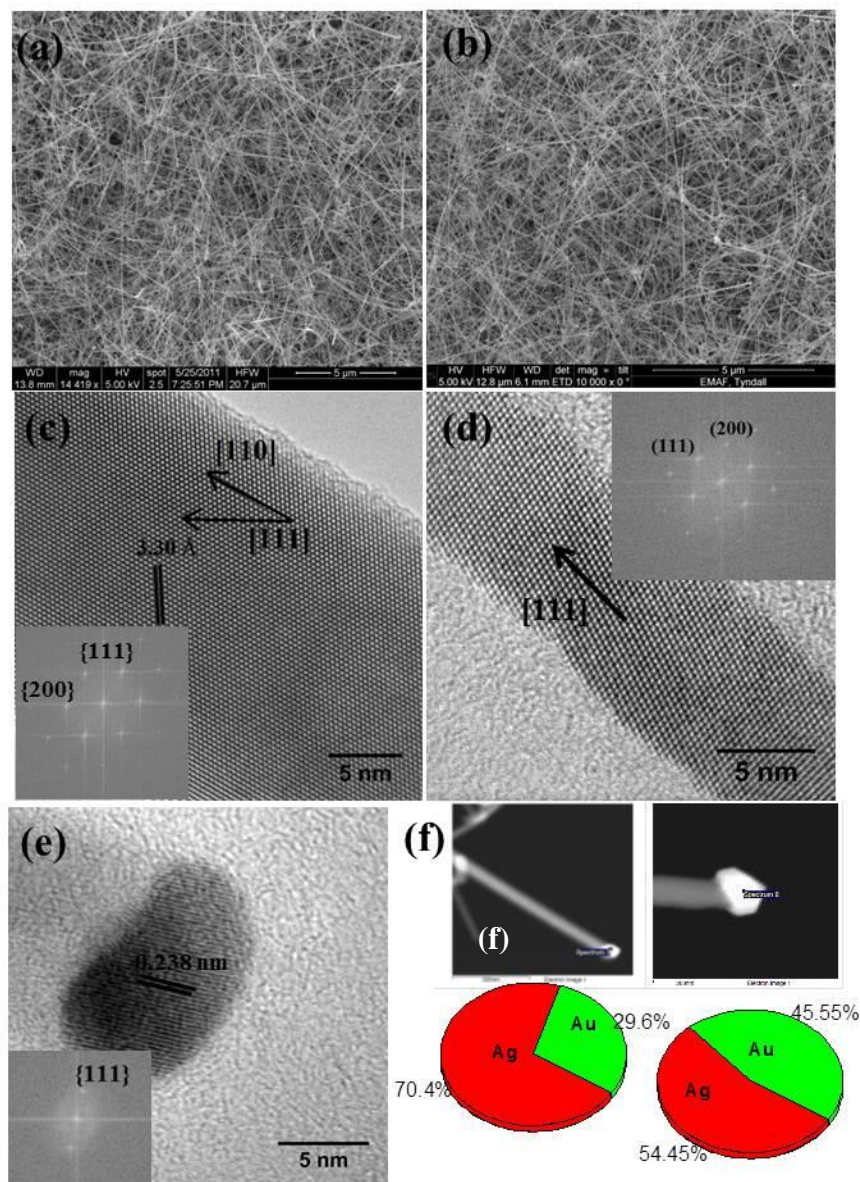


**Figure 2.** SEM images of Ge nanowires grown from 4 nm alloy particles: (a)  $\text{Ag}_{0.75}\text{Au}_{0.25}$  and (b)  $\text{Ag}_{0.50}\text{Au}_{0.50}$ . TEM images and corresponding FFT patterns showing (c)  $\langle 110 \rangle$  and (d)  $\langle 111 \rangle$  growth direction of nanowires. (e) TEM image and FFT (inset) of a metal tip at the end of a Ge nanowire, displaying fcc packing of the metal atoms. (f) Point EDX measurements taken from metal tips at the ends of Ge nanowires, indicating the Ag and Au stoichiometry in the  $\text{Ag}_{0.50}\text{Au}_{0.50}$  and  $\text{Ag}_{0.75}\text{Au}_{0.25}$  alloys.

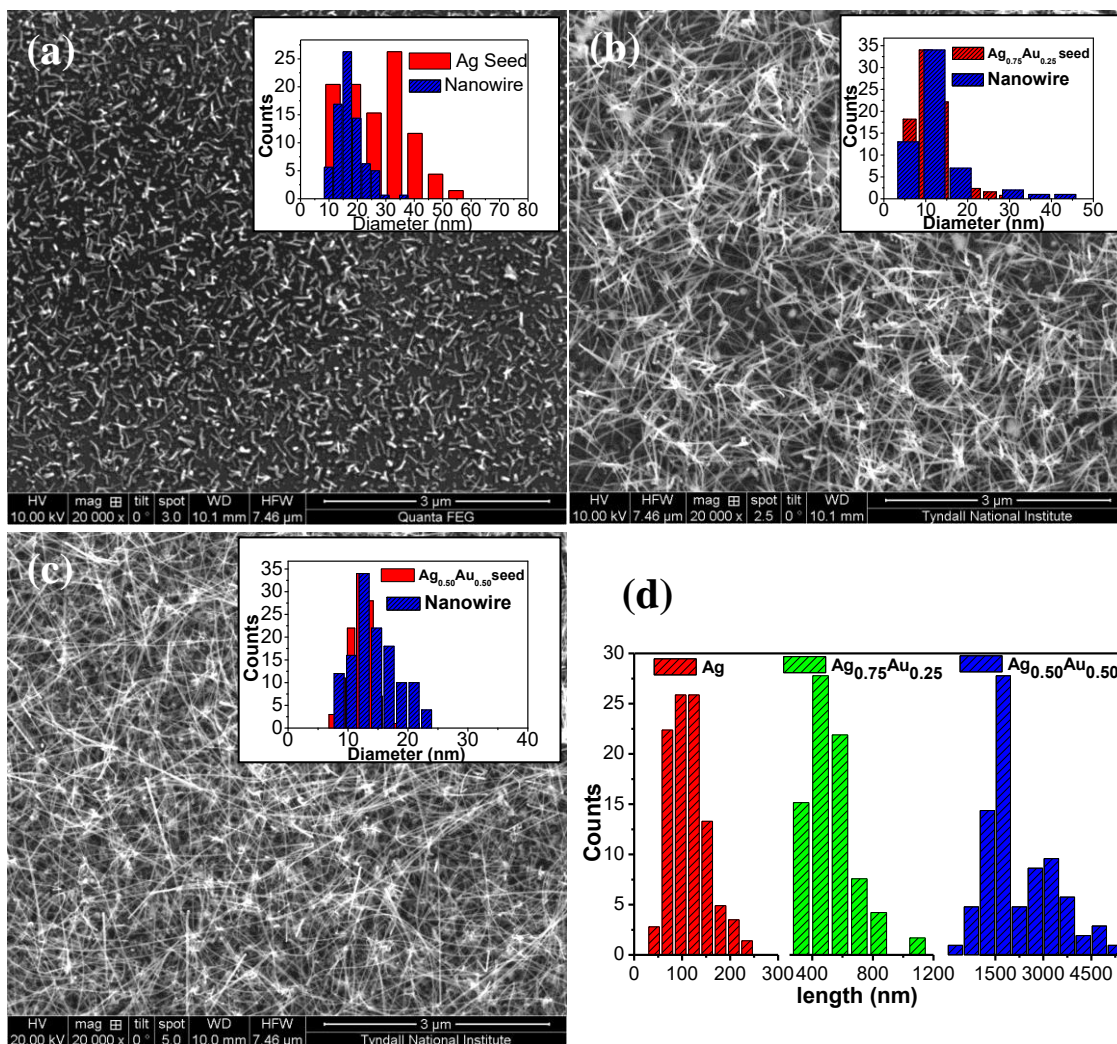


**Figure 3.** SEM images showing the different growth rate of Ge nanowires from (a) Ag, (b)  $\text{Ag}_{0.75}\text{Au}_{0.25}$  and (c)  $\text{Ag}_{0.50}\text{Au}_{0.50}$  nanoparticle seeds, after a 45 min growth time. Corresponding insets show the comparison of diameter distribution of nanowires (blue) and annealed growth seeds (red). The length distributions of the nanowires are shown in (d).

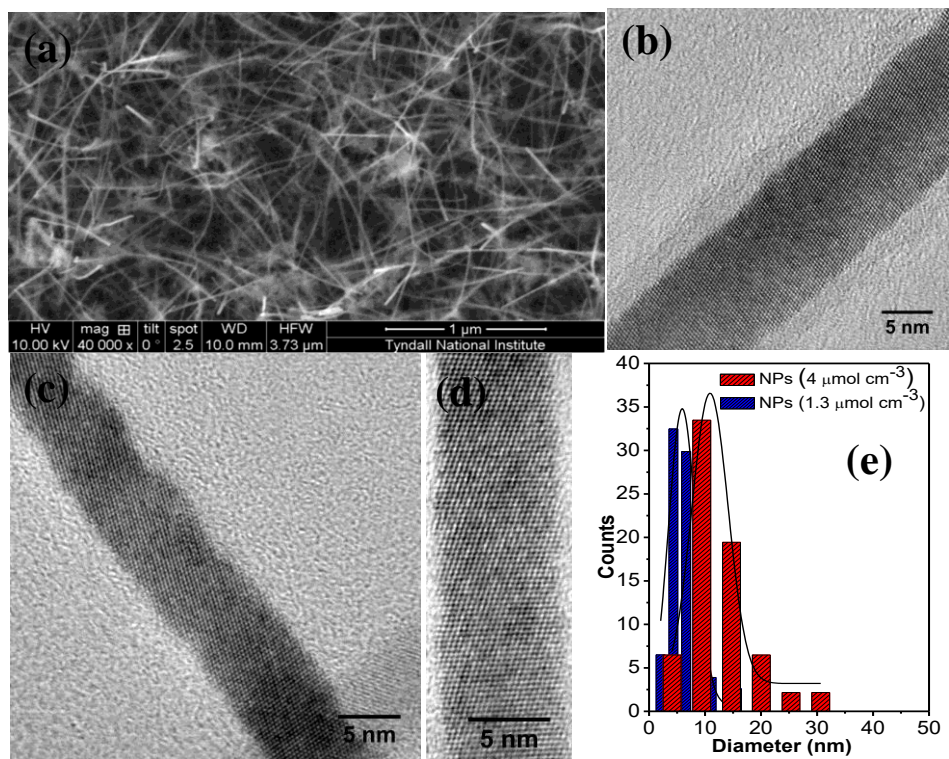


**Figure 4.** (a) SEM and (b)-(d) TEM images of super-thin nanowires grown using 2.5 nm  $\text{Ag}_{0.75}\text{Au}_{0.25}$  seeds. (e) Histograms showing the narrow diameter distributions for two different nanoparticle seed concentrations.

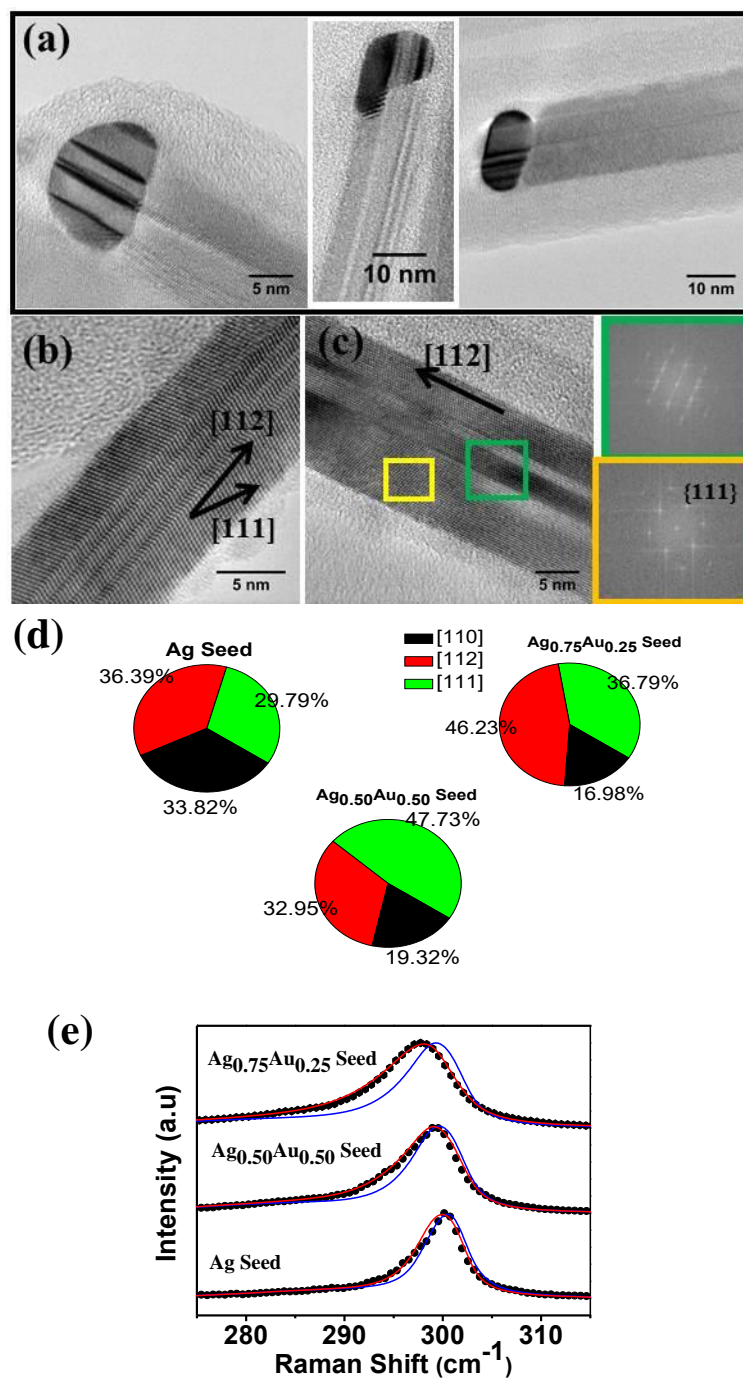


**Figure 5.** (a) TEM images displaying defect transfer from metal alloy seeds to Ge nanowires; identical brightness-contrast patterns between the nanoparticles and the nanowires can be observed. TEM images and FFT patterns of different nanowire segments in (b) and (c) illustrating the formation of  $\{111\}$  twin planes along  $\langle 112 \rangle$  growth axes. (d) Pie charts highlighting growth directions for Ag and  $Au_xAg_{1-x}$ -seeded Ge nanowires. (e) Raman spectra revealing the defect distributions for nanowires grown with different seeds; based on mismatches with the PCM fitted curves.